Charge-assisted hydrogen bond-directed self-assembly of an amphiphilic zwitterionic quinonemonoimine at the liquid-solid interface

Yuan Fang, Phuong Nguyen, Oleksandr Ivasenko, Maria Paola Aviles, Eskedar Kebede, Mohammad S. Askari, Xavier Ottenwaelder, Ulrich Ziener, Olivier Siri, and Louis Cuccia

SUPPORTING INFORMATION

1. Chemicals and Instrumentation

Chemicals 4,6-Diaminoresorcinol dihydrochloride, octadecylamine and 1,2,4-trichlorobenzene were obtained from Aldrich. Ethanol (anhydrous) was obtained from Fisher Scientific.Melting points (m.p.) were recorded with a capillary melting point apparatus (Thomas Hoover). The reported R_f values were determined by a standard thin-layer chromatography (TLC) procedure: 0.25 mm silica gel plates eluted with chloroform/methanol (98:2).

NMR ^{1}H NMR (500 MHz) and ^{13}C NMR (125 MHz) spectra were recorded on a Varian 500 spectrometer at ambient temperature. The residual proton and carbon signals of deuterated $CHCl_3$ were used as internal standards ($CDCl_3$: δ (^{1}H) 7.26 ppm, δ (^{13}C) 77.23 ppm). The following notation is used for the ^{1}H NMR splitting patterns: singlet (s), doublet (d), triplet (t), quartet (q), quintet (p), multiplet (m) and broad signal (br).

MS Mass spectrometric analysis was performed using a Waters Micromass, Quattro LC triple quadrupole mass spectrometer (Waters, Montreal, PQ, Canada). The instrument was operated using an ESI (electrospray ionization) source by direct injection with a syringe pump (50 µL syringe; flow rate: 1 µL/min). The MS instrument was operated in the positive mode (ES+) and the data acquisition/analysis was carried out using Masslynx software version 4.01. Source working conditions were as follows: cone voltage: 20 V, Capillary voltage: 3.3 V, source temperature: 90 °C, desolvation temperature: 100 °C, desolvation gas flow rate: 220 L/hr, nitrogen: (99.9% purity, from cylinder).

UV-Vis UV-Vis spectra were recorded on an Agilent 8453 UV-Visible spectrophotometer.

STM STM measurements were carried out under ambient conditions with a Bruker Nanoscope MultiMode Scanning Probe Microscope equipped with a low-current STM head or an RHK STM (SPM1000) running under ambient conditions. *In situ* STM imaging was performed at the liquid/solid interface; the substrate was freshly cleaved highly oriented pyrolytic graphite (HOPG; ZYB quality; NT-MDT Castletroy, Limerick, Ireland). Mechanically sharpened Pt/Ir (90/10 or 80/20; NanoScience Instruments, Phoenex, AZ) tips were tested by obtaining atomic resolution images of graphite and subsequently a drop (*ca.* 5 µL) of **C18Q** in 1,2,4-trichlorobenzene was added. Self-assembled monolayers (SAMs) were observed immediate after the tip was engaged. The concentration of **C18Q** was typically close to saturation, but lower concentrations also led to the same molecular packing.

The specific tunneling conditions are given in the figure captions. Images in Figures SI-4a, SI-4b and SI-6 were flattened and Gaussian smoothed using WSxM[1] software and the images in Figures SI-4a and SI-6 have been lattice-corrected for distortion due to drift. All other images were flattened and median filtered using the Nanoscope 6.14r2 software. The unit cell of **C18Q** was measured based on 17 lattice-corrected images and the overall error in the unit cell was determined to be below 4%.

2. Synthesis and characterization of C18Q:

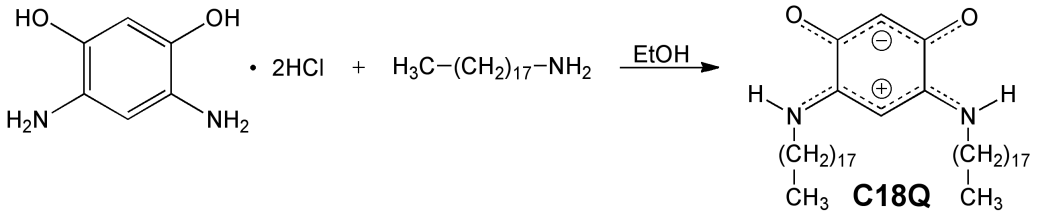

4,6-Diaminoresorcinol dihydrochloride (110.4 mg; 0.518 mmol) was dispersed in ethanol (7 mL) and after 2 min. octadecylamine (1.1014 g; 4.086 mmol) was added to the stirred solution. The mixture was left to stir for *ca.* one day. The resulting dark green precipitate was isolated by vacuum filtration on filter paper, washed with cold ethanol and air-dried. The crude product was purified by centrifugal chromatography on silica (98/2 chloroform/methanol) and dried under vacuum (259.7 mg; 0.404 mmol; 78%). Single crystals suitable for X-ray diffraction were obtained by slow evaporation from $CDCl_3$. m.p. 105.5-107.0 °C; R_f 0.35 (98/2 $CHCl_3$/MeOH); ^{1}H NMR (500 MHz, $CDCl_3$) δ 0.88 (t, ^{3}J = 7.0 Hz, 6H, CH_3), 1.26 (m, 56H, CH_2-CH_2-CH_2), 1.73 (p, ^{3}J = 7.3 Hz, 4H, NH-CH_2-CH_2), 3.37 (dt, ^{3}J = 6.7 Hz, 4H, NH-CH_2), 5.13 (s, 1H, NH-C-C*H*), 5.44 (s, 1H, O-C-C*H*), 8.32 (br s, 2H, N*H*); ^{13}C NMR (125 MHz, $CDCl_3$): δ 14.08 (CH_3), 22.66, 26.92, 28.27, 29.14, 29.33, 29.41, 29.52, 29.60, 29.63, 29.67, 31.90, 43.30, 80.53 (N-C-*C*), 98.81 (O-C-*C*), 156.61 (N-*C*), 172.33 (O-*C*); UV-Vis: λ 337 (log ε = 4.41), 350 (log ε = 4.43); MS (Triple Quad-ESI): m/z: 643.65 $[M+H]^+$ calcd $[M+H]^+$: 644.08

3. Alternative structure of C18Q surface self-assembly

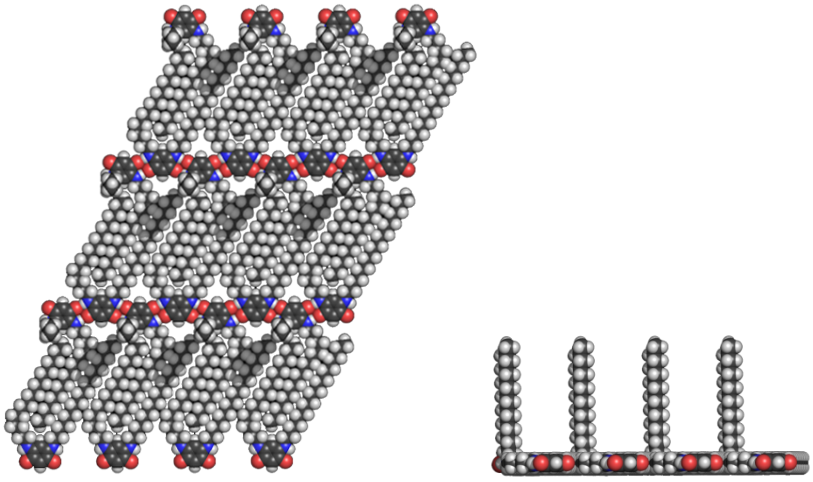

Figure SI-1. Alternative packing model of **C18Q** with an alkyl chains pointing out of the plane of the monolayer; top view (left) and side view (right).

4. Packing and favorable van der Waals interactions between the alkyl chains of a C18Q monolayer.

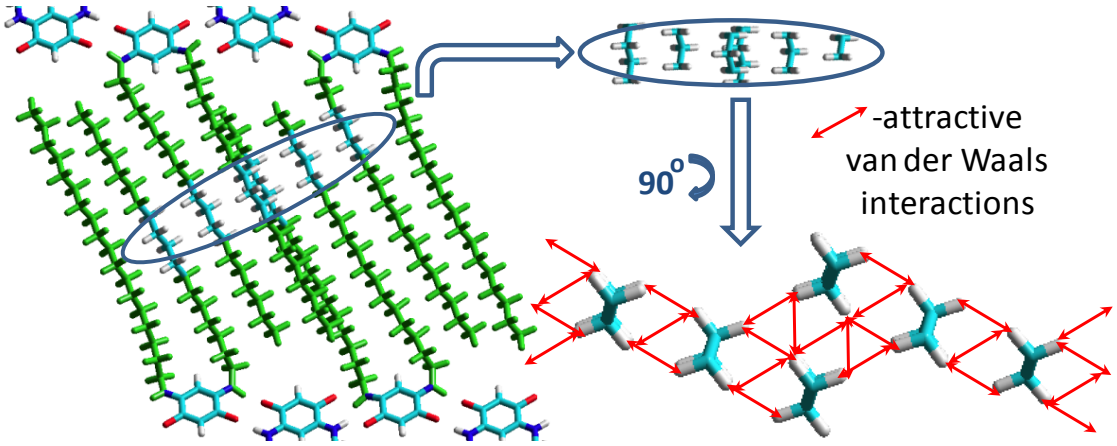

Figure SI-2. Schematic representation of multiple van der Waals interactions between the alkyl chains of a **C18Q** monolayer. Here we have used a small C18Q cluster where all aromatic cores were frozen at experimentally observed distances while alkyl chains within lamella were allowed to relax using general force field MM+ implemented in HyperChem 7.5 (Copyright 2002; HyperChem, v. 7.5; HyperCube Inc.; Gainesville, FL.)

5. Periodicity of the alkyl chains of C18Q

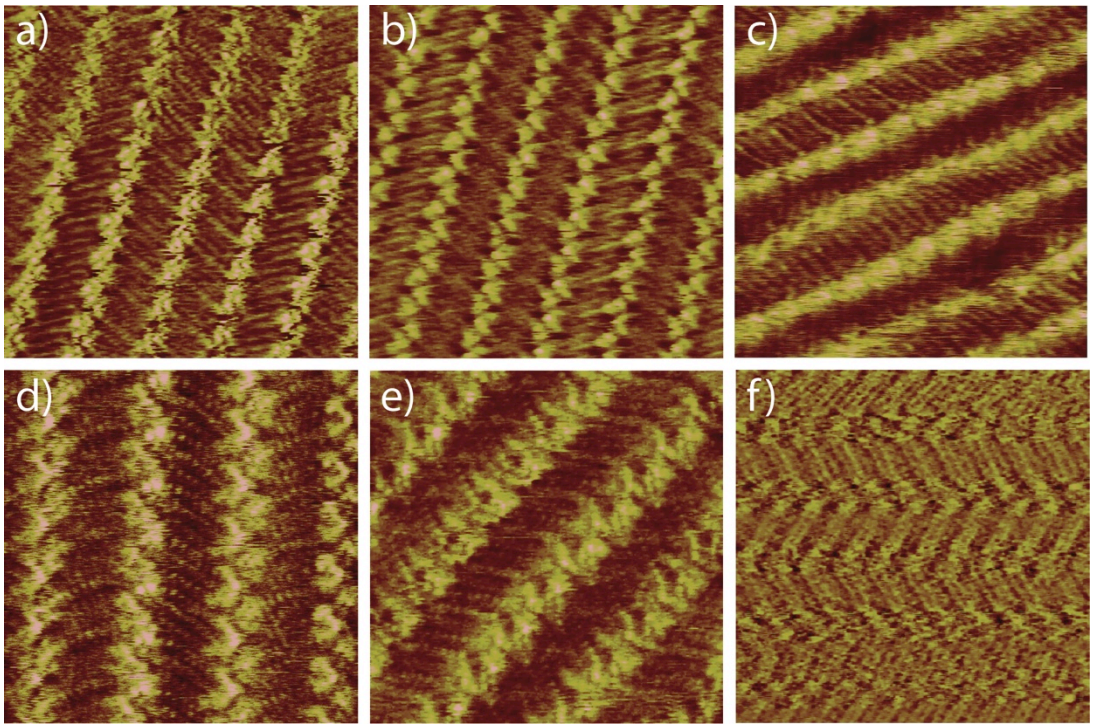

Figure SI-3. STM topography images (a-e) and current image (f) of C18Q where the periodicity of every third alkyl chain is observed. (a) 15 nm × 15 nm; It = 17.3 pA, Vb = -522.7 mV; (b) 15 nm × 15 nm; It = 17.3 pA, Vb = -322.9 mV; (c) 15 nm × 15 nm; It = 40.0 pA, Vb = -300 mV; (d) 10 nm × 10 nm; It = 16.0 pA, Vb = -500 mV; (e) 10 nm × 10 nm; It = 22.0 pA, Vb = -485.2 mV and (f) 20 nm × 20 nm; It = 18.7 pA, Vb = -734.9 mV.

6. Calculated Moiré pattern

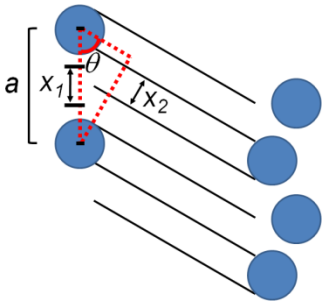

Graphite periodicity = 2.46 Å
Periodicity of the zig-zag rows (a) = 14.8 Å
Distance between alkyl chains along the headgroup axis (x_1) = 14.8 Å /3 = 4.93 Å
Angle between alkyl chains and head group rows (θ) = 60°
Perpendicular alkyl chain periodicity (x_2) = 4.93 Å x sin(60°) = 4.27 Å
Calculated Moiré pattern = 4 chains

7. The difference in free energies of herringbone and linear assemblies

107 pairwise alkyl chain observations were tabulated and 15 linear and 92 herringbone arrangements were observed in 19 distinct images of **C18Q**. This corresponds to 86% of herringbone and 14% of linear arrangements.

$\Delta G = -RT\ln K$ = -8.314 x 298 x ln(86/14)=-4497.5 J/mol, or ~1 kcal/mol

8. The role of the substrate in the packing of C18Q.

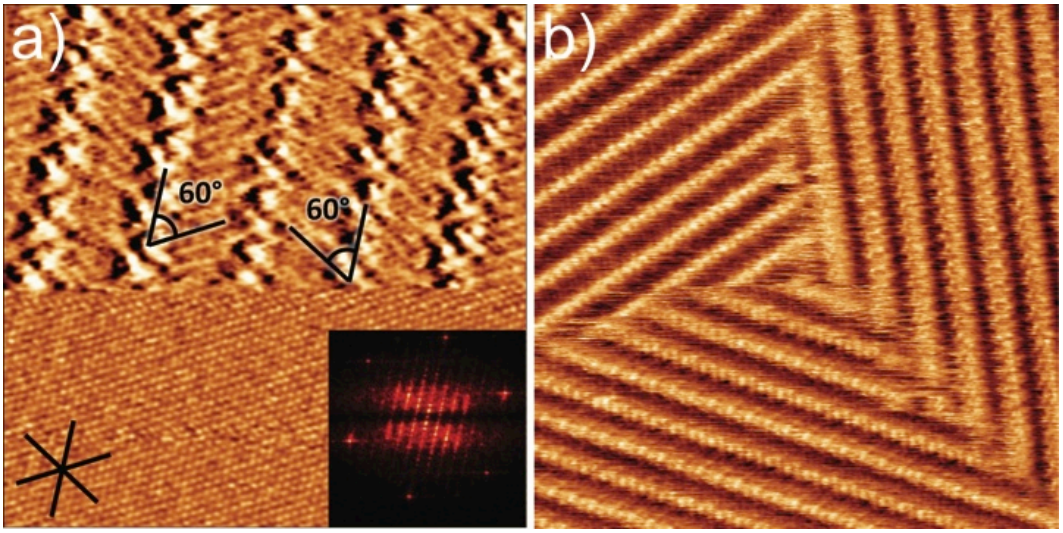

Figure SI-4. (a) STM current image of C18Q at the TCB/HOPG interface. The current was changed during scanning, revealing atomic resolution of the HOPG. The angle between alkyl chains and head groups is 60 ± 2°. 15 nm × 15 nm; I_t = 17.3 pA. V_b = -322.9 mV (SAM). I_t = 17.3 pA, V_b = 40 mV (HOPG). Inset: 2D Fast Fourier Transform indicates that head group rows of C18Q follow one of the main axes of HOPG. (b) STM topography image of C18Q at the TCB/HOPG interface. 43 nm × 43 nm; I_t = 1.26 pA, V_b = -433 mV.

9. Origin and structure of C18Q bilayers.

The most stable structure of bilayer is the one with parallel arrangement of lamellae in both layers which is expected to maximize favorable van der Waals interactions (Figure SI-3). 'Criss-cross' bilayer is simply the result of continuous growth of the second layer over multi-domain region of the first layer in which all domains are rotated by 60° with respect to each other (Figure SI-4a & SI-4b).

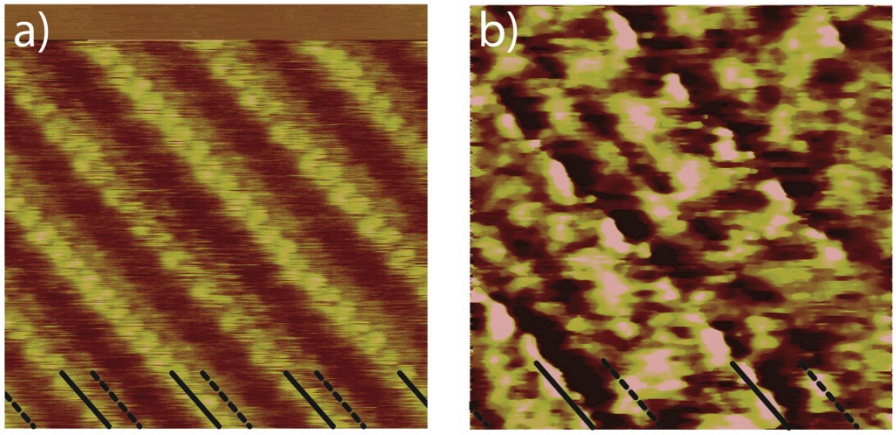

Figure SI-5A. STM topography images of **C18Q** at the HOPG/TCB interface showing offset parallel bilayers. Dashed arrows point to the lower layer and solid arrows point to the top layer. (a) 15 nm × 15 nm; I_t = 20.0 pA, V_b = -518.8 mV and (b) 10 nm × 10 nm; I_t = 20.3 pA, V_b = -96.6 mV.

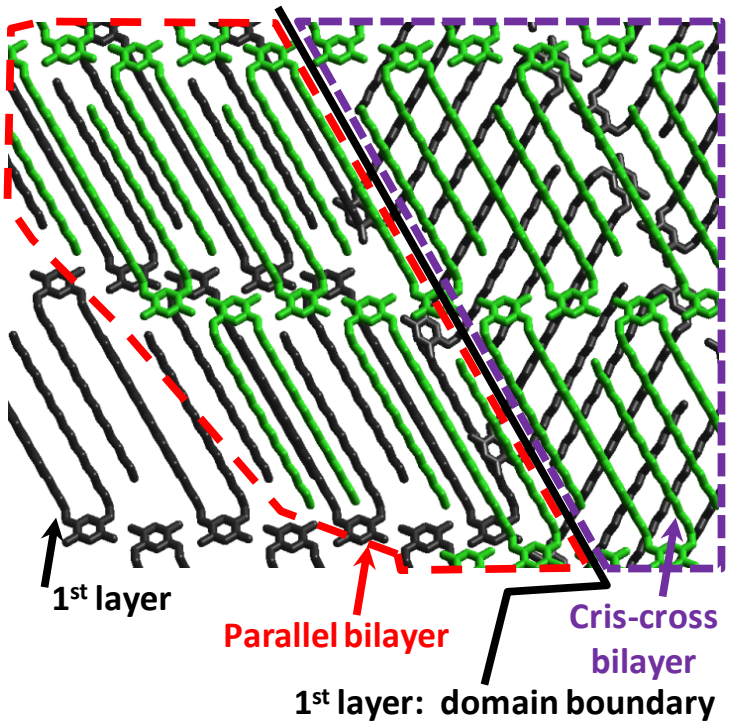

Figure SI-5B. A schematic model illustrating the formation and structure of criss-cross bilayers. This observation suggests that penalties for both breaking intermolecular interactions within the second layer and creating domain boundaries complementary to the layer underneath seems to be higher than the energy difference between parallel and criss-cross interlayer configurations.

10. X-ray structure and crystallographic data

A red plate-like specimen of **C18Q** ($C_{43}H_{81}Cl_3N_2O_3$), approximate dimensions 0.070 mm x 0.100 mm x 0.120 mm, was used for the X-ray crystallographic analysis. The X-ray intensity data were measured on a Bruker SMART APEX II CCD system equipped with a Cu ImuS microfocus source with QUAZAR optics (λ = 1.54178 Å). A total of 7320 frames were collected. The total exposure time was 20.33 hours. The frames were integrated with the Bruker SAINT software package using a narrow-frame algorithm. The integration of the data using a triclinic unit cell yielded a total of 45090 reflections to a maximum θ angle of 68.16° (0.83 Å resolution), of which 15653 were independent (average redundancy 2.881, completeness = 94.1%, R_{int} = 4.64%, R_{sig} = 5.33%) and 9911 (63.32%) were greater than $2\sigma(F^2)$. The final cell constants of a = 9.53790(10) Å, b = 15.4567(2) Å, c = 31.2770(4) Å, α = 80.4140(10)°, β = 89.3420(10)°, γ = 87.0510(10)°, volume = 4540.57(10) $Å^3$, are based upon the refinement of the XYZ-centroids of 9965 reflections above 20 σ(I) with 5.731° < 2θ < 135.0°. Data were corrected for absorption effects using the multi-scan method (SADABS). The ratio of minimum to maximum apparent transmission was 0.920. The calculated minimum and maximum transmission coefficients (based on crystal size) are 0.7788 and 0.8615. The structure was solved and refined using the Bruker SHELXTL Software Package, using the space group P -1, with Z = 4 for the formula unit, $C_{43}H_{81}Cl_3N_2O_3$. The final anisotropic full-matrix least-squares refinement on F^2 with 956 variables converged at R1 = 5.20%, for the observed data and wR2 = 14.13% for all data. The goodness-of-fit was 1.014. The largest peak in the final difference electron density synthesis was 0.459 $e^-/Å^3$ and the largest hole was -0.380 $e^-/Å^3$ with an RMS deviation of 0.047 $e^-/Å^3$. On the basis of the final model, the calculated density was 1.142 g/cm^3 and F(000), 1712 e^-.

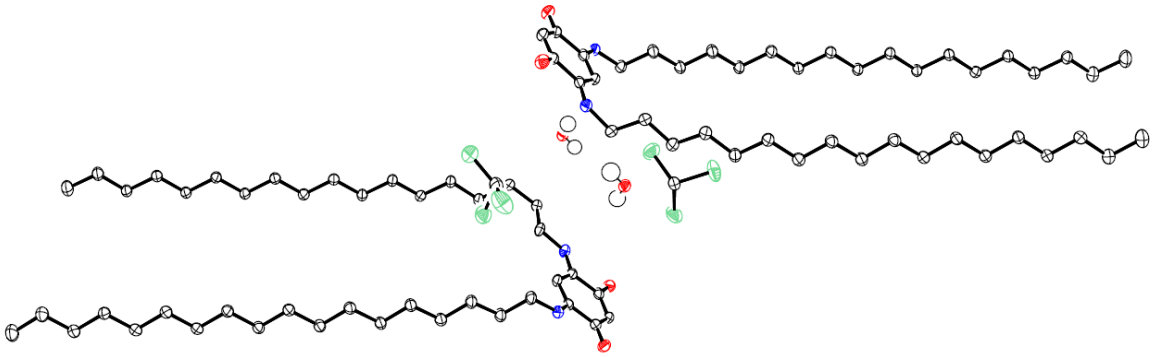

Figure SI-6. Crystal structure of **C18Q** at 50% ellipsoid probability.

Table SI-1: Crystal data and structure refinement for **C18Q**

Empirical formula	$C_{42}H_{78}N_2O_2 \cdot CHCl_3 \cdot H_2O$	
Formula weight	780.45	
Temperature	116(2) K	
Wavelength	1.54178 Å	
Crystal system	Triclinic	
Space group	P(-1)	
Unit cell dimensions	*a* = 9.53790(10) Å	α = 80.4140(10)°
	b = 15.4567(2) Å	β = 89.3420(10)°
	c = 31.2770(4) Å	γ = 87.0510(10)°
Volume	4540.57(10) $Å^3$	
Z	4	

Density (calculated)	1.142
Absorption coefficient	2.105
F(000)	1712
Crystal size	0.12 × 0.10 × 0.07 mm
Theta range for data collection	1.43 – 68.16
Index ranges	$h = -11 \rightarrow 11$, $k = -16 \rightarrow 18$, $l = -37 \rightarrow 37$
Reflections collected	45090
Independent reflections	15653
Completeness to theta = 68.16°	94.1%
Absorption correction	Multiscan
Refinement method	Full-matrix least-squares on F^2
Data / restraints / parameters	15653 / 0 / 955
Goodness of fit on F^2	1.014
Final R indices [I > 2σ(I)]	R_1 = 5.20%, wR_2 = 12.05%
R indices (all data)	R_1 = 9.31%, wR_2 = 14.13%
Largest diff. peak and hole	0.46 and -0.38 e $Å^{-3}$

11. General

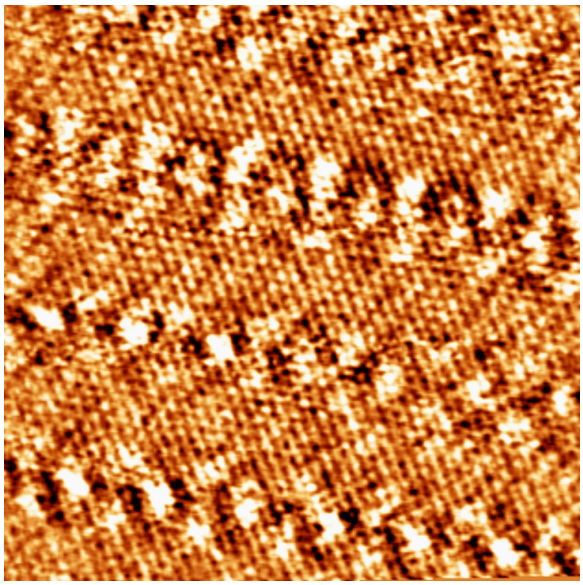

Figure SI-7. STM topography images of **C18Q** at the HOPG/TCB interface under ambient conditions. The molecular orientation is superposed on a resolved graphite lattice. This image reveals the molecular orientation with respect to HOPG. 10 nm × 10 nm; I_t = 23.3 pA, V_b = 581.2 mV.

References:

1. I. Horcas, R. Fernández, J. M. Gómez-Rodríguez, J. Colchero, J. Gómez-Herrero and A. M. Baro, *Rev. Sci. Instrum.*, 2007, **78**, 013705-1 - 013705-8.